Using Steady-State Response for Predicting Stability Boundaries in Switched Systems Under PWM with Linear and Bilinear Plants

A. El Aroudi, M. Al-Numay, K. Al Hosani and N. Al Sayari

Abstract Switching systems under Pulse Width Modulation (PWM) are commonly utilized in many industrial applications. Due to their associated nonlinearities, such systems are prone to exhibit a large variety of complex dynamics and undesired behaviors. In general, slow dynamics in these systems can be predicted and analyzed by conventional averaging procedures. However, fast dynamics instabilities such as period doubling (PD) and saddle-node (SN) bifurcations cannot be detected by average models and analyzing them requires the use of additional sophisticated tools. In this chapter, closed-form conditions for predicting the boundary of these bifurcations in a class of PWM systems with linear and bilinear plants are obtained using a time-domain asymptotic approach. Previous studies have obtained similar boundaries by either solving the eigenvalue problem of the monodromy matrix of the Poincaré map or performing a Fourier series expansion of the feedback signal. While the former approach is general and can be applied to linear as well as bilinear plants, the later approach is applicable only to PWM systems with linear plants. The conditions for fast scale instability boundaries presented in this chapter are obtained from the steady-state analysis of the Poincaré map using an asymptotic approach without resorting to frequency-domain Fourier analysis and without using the monodromy matrix of the Poincaré map. The obtained expressions are simpler than the previously reported ones and allow to understand the effect of different system's

A. El Aroudi (✉)
University Rovira i Virgili, Tarragona, Spain
e-mail: abdelali.elaroudi@urv.cat

M. Al-Numay
King Saud University, Riyadh, KSA
e-mail: alnumay@ksu.edu.sa

K. Al Hosani · N. Al Sayari
The Petroleum Institute, Abu Dhabi, UAE
e-mail: khalhosani@pi.ac.ae

N. Al Sayari
e-mail: nalsayari@pi.ac.ae

M. Belhaq (ed.), *Structural Nonlinear Dynamics and Diagnosis*,
Springer Proceedings in Physics 168, DOI 10.1007/978-3-319-19851-4_18

parameters on its stability. In PWM systems with linear plants, under certain practical conditions concerning these parameters, the matrix form expression can be approximated by standard polynomial functions expressed in terms of the operating duty cycle weighted by the Markov parameters of the linear part of the system.

1 Introduction

Switched systems constitute a special class of nonlinear dynamical systems [1] and arise often in many practical engineering systems when some switching elements such as switches or diodes, block with dead-zone, saturated amplifiers, relays and comparators in electrical systems are present. This is also the case of mechanical systems where impacts or nonsmooth friction take place. A particular class of switched systems are those characterized by linear differential equations between switching events. These systems are called therefore piecewise linear (PWL) or piecewise affine (PWA) systems [2]. Most of the PWL systems studied in the literature are characterized by switching among linear subsystems when certain time-varying and T—periodic boundaries in the state-space are reached. This is the case of Pulse Width Modulation (PWM) systems like switching DC-DC power converters [3–8], DC-AC inverters [9], temperature control systems [10], switched capacitor networks and chaos generators [11] and hydraulic and fluid valve drivers [12, 13]. Nonlinearity arises from the feedback which imposes a constraint relating the duty cycle nonlinearly and in general implicitly to the vector of the system state variables. Despite their engineering use, one of the main drawbacks of switched systems under PWM is this nonlinearity making them prone to exhibit a large variety of complex dynamics and undesired behaviors [6, 10, 11]. Although each subsystem is linear and its describing differential equations can be solved in closed-form, the dynamics of the complete switched system is highly nonlinear and its accurate stability analysis requires sophisticated computational tools [14].

Switched systems under PWM employ switching devices to control a suitable output variable by using a T—periodic external modulating signal. Therefore, the only acceptable nominal operation of any switched system under PWM is a T—periodic oscillation around the desired level. When the stability of this periodic operation is lost, different slow scale-time or fast scale-time nonlinear phenomena can take place [15].

The dynamical behavior and the accurate stability analysis of this kind of systems can either be tackled by long-time integration of the continuous-time switched model, discrete-time model and its Jacobian matrix or Floquet theory with Fillipov technique to compute the mondromy matrix [16]. Other methods leading to the same matrix and based on trajectory sensitivity analysis are also available [17]. After obtaining the Jacobian or monodromy matrix, critical boundary conditions for some singularities like saddle-node (SN) bifurcation or period-doubling (PD) can be obtained by imposing that one eigenvalue is equal to $+1$ or -1, respectively [4]. It is in general

very cumbersome to compute the stability boundary of a PWM system using the previous methods.

Another approach, which was called *harmonic balance*,[1] used for the first time in [18] and recently in [5] for locating these boundaries is by expanding the feedback signal into a Fourier series to obtain the steady-state trajectory in certain periodic regimes and imposing critical conditions for the occurrence of the corresponding singularities like PD and SN bifurcations.

The conditions for fast scale instability boundaries presented in this chapter are obtained from the steady-state analysis of the Poincaré map using a time domain asymptotic approach without resorting to frequency-domain Fourier analysis and without using the monodromy matrix of the Poincaré map. The obtained expressions are simpler than the previously reported ones and allow to understand the effect of different system's parameters on its stability. Examples of PWM systems that can be studied by the approach of this chapter are DC-DC switching power electronics converters [3, 5, 6], DC-AC inverters [9], temperature control systems [10] and switched capacitor chaos generators [11], among others.

The rest of the chapter is organized as follows. Section 2 presents the switched model of systems with bilinear plants under PWM. A review of Poincaré map modeling approach is explained in Sect. 3 together with its steady-state solution. Subsequently, Sect. 4 deals with the steady-state approach for predicting the boundary of SN and PD instabilities in this kind of systems by imposing boundary conditions in the time-domain on the steady-state T-periodic and the $2T$—periodic orbits together with their respective switching conditions imposed by the PWM process. Finally, some concluding remarks are drawn in the last section.

2 Bilinear Modeling of PWM Switched Systems

2.1 Pulse Width Modulation

Pulse-width modulation is a technique used, among others, to control switched systems. This modulation technique is one of the mostly used methods in switched mode power supply for different applications. In this kind of systems, the average value of voltage or current fed to the load is controlled by turning ON and OFF some switching devices such as MOSFETs and IJBTs. The PWM switching frequency has to be much higher than the time constants of the plant to be controlled to minimize the ripple of the voltage or current applied to the load. The term duty cycle is defined as the proportion of ON-time duration of the switching element to the complete switching period. In the traditional PWM strategy, the duty cycle of the pulse driving signal $u(t)$ is varied according to the control signal $x_c(t)$ which correspond to

[1] In [5] this type of analysis was called *Harmonic Balance*. Here this term was conserved but to the opinion of the authors only a steady-state analysis of the feedback signal expressed in Fourier series has been used and no harmonic balance has been performed since the system loop is linear.

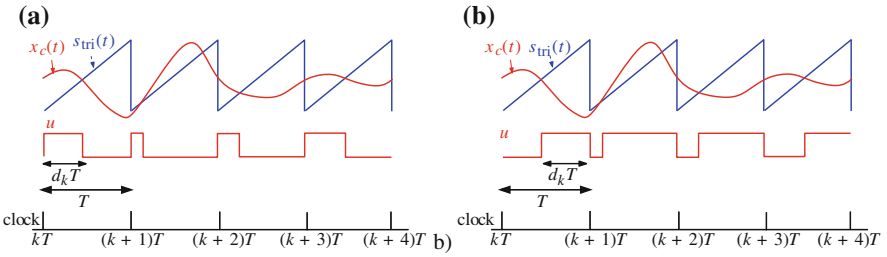

Fig. 1 Waveforms of the T—periodic external signal $s_{\text{tri}}(t)$ and the control signal **a** TEM $x_c = \mathbf{C}^{\intercal}(\mathbf{X}_{\text{ref}} - \mathbf{x}(t))$, **b** LEM $x_c = \mathbf{C}^{\intercal}(\mathbf{x}(t) - \mathbf{X}_{\text{ref}})$

a compensated version of the error between the output variable (voltage or current) and its desired reference x_{ref}. This error is processed through an error compensator to provide the control signal $x_c(t)$. In direct duty cycle control, the simplest analog form of generating a fixed frequency PWM is by comparing the control voltage with a ramp periodic signal $s_{\text{tri}}(t)$ in such a way that the pulse signal $u(t)$ goes high/low at switching instants t_s when the control signal $x_c(t)$ is higher/lower than the triangular signal $s_{\text{tri}}(t)$ (Fig. 1). In other constant frequency modulation schemes, the switch is turned ON (resp. OFF) periodically while it is turned OFF (resp. ON) whenever the peak (resp. valley) control signal x_c reaches the ramp compensator. The ratio of the first interval duration $t_{s,k}$ to the complete period T $((t_{s,k})/T)$ during the switching cycle $(kT, (k+1)T)$ is the duty cycle d_k in that cycle for Trailing Edge Modulation (TEM) strategies while it is its complementary $\overline{d}_k = 1 - d_k$ for Leading Edge Modulation (LEM) strategies. The control signal for TEM strategies can be expressed as $x_c = \mathbf{C}^{\intercal}(\mathbf{X}_{\text{ref}} - \mathbf{x})$ while it is $x_c = \mathbf{C}^{\intercal}(\mathbf{x} - \mathbf{X}_{\text{ref}})$ for LEM schemes, where $\mathbf{x} \in \mathbb{R}^n$ is the vector of the state variables including the power stage and the controller parameters and n is the order of the system after excluding any existing integrator in the loop. $\mathbf{C}$ is an appropriate feedback vector and $\mathbf{X}_{\text{ref}}$ is a suitable reference vector. In both strategies, the generation of the PWM driving signal is carried out by comparing the control signal x_c with the T—periodic signal s_{tri}.

2.2 The Bilinear Switched Model

Let us focus on TEM strategy. The results corresponding to LEM can be deduced from those of TEM strategy by just a change of variable $d_k \to 1 - d_k$. During a switching period of length T, an orbit of a switched system under PWM starting at time instant kT $(k \in \mathbb{Z})$ is forced, using a clocked latch, to be governed by the vector field

$$\mathbf{f}_1(\mathbf{x}, \mathbf{w}) = \mathbf{A}_1\mathbf{x} + \mathbf{B}_1\mathbf{w} \tag{1}$$

This orbit intersects with a switching boundary, at a certain switching instant $t_s = d_kT$ decided by the modulation strategy. The switching occurs when the external

periodic ramp signal s_{tri} intersects with the control signal x_c. The orbit then goes to another different linear system described by the vector field

$$\mathbf{f}_2(\mathbf{x}, \mathbf{w}) = \mathbf{A}_2\mathbf{x} + \mathbf{B}_2\mathbf{w} \tag{2}$$

where $\mathbf{A}_i \in \mathbb{R}^{n\times n}$ and $\mathbf{B}_i \in \mathbb{R}^{n\times m}$, $i = 1, 2$ are the system state matrices for phase i and $\mathbf{w} \in \mathbb{R}^m$ is the vector of the external parameters of the plant and controller, m being the number of the external inputs to the system which are supposed to be constant within a switching cycle. The system is forced periodically and synchronously to the first phase ($i = 1$) characterized by the vector field $\mathbf{f}_1$ while it is switched to the second phase ($i = 2$) characterized by the vector field $\mathbf{f}_2$ whenever the condition $\sigma(\mathbf{x}, t) := \mathbf{C}^\intercal(\mathbf{X}_{\text{ref}} - \mathbf{x}) - s_{\text{tri}} = 0$ holds. In compact form, the model of a switched system under PWM can be written in the following general *bilinear* form

$$\dot{\mathbf{x}} = u\mathbf{f}_1(\mathbf{x}, \mathbf{w}) + (1 - u)\mathbf{f}_2(\mathbf{x}, \mathbf{w}) \tag{3a}$$

where $\mathbf{f}_1(\mathbf{x}, \mathbf{w}) = \mathbf{A}_1\mathbf{x} + \mathbf{B}_1\mathbf{w}$, $\mathbf{f}_2(\mathbf{x}, \mathbf{w}) = \mathbf{A}_2\mathbf{x} + \mathbf{B}_2\mathbf{w}$ and $u \in \{0, 1\}$ is the driving signal which is generated by the PWM process by which the system is forced to one phase cyclically while it is switched to the other phase whenever the control signal x_c crosses the periodic signal $s_{\text{tri}}(t)$. In TEM strategies, the switching condition $\mathbf{C}^\intercal(\mathbf{X}_{\text{ref}} - \mathbf{x}) = s_{\text{tri}}$ can be written as $-\mathbf{C}^\intercal\mathbf{x} = r$, where $r = -\mathbf{C}^\intercal\mathbf{X}_{\text{ref}} + s_{\text{tri}}$.

3 Review of Poincaré Map Modeling of PWM Systems

3.1 Closed-Form Solution of the State Variables

The trajectory $\mathbf{x}(t)$ at time t of the system starting from an initial condition $\mathbf{x}(t_0)$ at time instant t_0 can be expressed as follows

$$\mathbf{x}(t) = e^{\mathbf{A}_i(t-t_0)}\mathbf{x}(t_0) + \mathbf{A}_i^{-1}(e^{\mathbf{A}_i(t-t_0)} - \mathbf{I})\mathbf{B}_i\mathbf{w} \tag{4}$$

It is assumed that the matrix $\mathbf{A}_i$ is nonsingular. It should be noted that two kinds of singularities may arise in this kind of switched systems which are detailed below:

1. A singularity which takes place only theoretically and that can be avoided by just adding parasitic elements [19].
2. A structural singularity that cannot be avoided by just adding parasitics. In this case, the previous expression for the solution of the system state variables cannot be used if the integrator was taken into account despite the fact that this solution exists and it is well defined even in the case when the matrix $\mathbf{A}_i$ is not invertible. However, the integral action has no meaning without closing the loop by the feedback and the PWM process. Having said that, the switched model used in this study and the expression of the trajectories in (4) do not take into account the

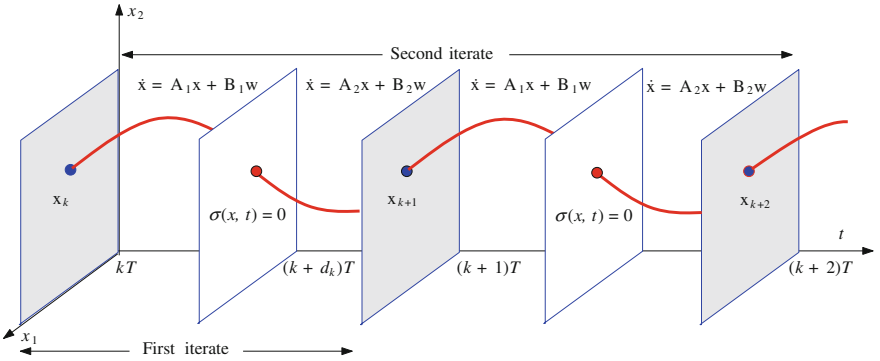

Fig. 2 State-space representation of a switched system under PWM

integral variable. However, while the integral action could have an effect on the slow scale dynamics, its effect on the fast scale dynamics is negligible [6].

3.2 Local Mappings

Since the vector fields between the switching events are linear we can use the exact analytical solution to express the value of the state vector at the end of a switching cycle in terms of its value at the beginning of that cycle, Fig. 2. The local Poincaré map of the system within switching sub-intervals can be obtained by using (4) during the corresponding interval [2]. Let us define $\mathbf{x}_k = \mathbf{x}(kT)$, $\mathbf{x}_d = \mathbf{x}((k + d_k)T)$, $\mathbf{x}_{k+1} = \mathbf{x}((k + 1)T)$ where d_k is the duty cycle during the cycle $(kT, (k + 1))T$. Therefore, the local mappings are given by

$$\mathbf{x}_d := P_1(\mathbf{x}_k) = \mathbf{\Phi}_1(d_kT)\mathbf{x}_k + \mathbf{\Psi}_1(d_kT) \tag{5a}$$

$$\mathbf{x}_{k+1} := P_2(\mathbf{x}_d) = \mathbf{\Phi}_2((1 - d_k)T)\mathbf{x}_d + \mathbf{\Psi}_2((1 - d_k)T) \tag{5b}$$

where, according to (5a) and (5b), $\mathbf{\Phi}_k(t)$ and $\mathbf{\Psi}_k(t)$ are defined by:

$$\mathbf{\Phi}_k(t) = e^{\mathbf{A}_k t} \quad \text{and} \quad \mathbf{\Psi}_k(t) = \mathbf{A}_i^{-1}(e^{\mathbf{A}_i t} - \mathbf{I})\mathbf{B}_i\mathbf{w} \tag{6}$$

Most parts of this chapter require only a very moderate knowledge of mathematics. What is importantly required is just an understanding of the previous solution and simple algebraic matrix arrangements as it will be shown later.

3.3 Linear Poincaré Map for the Open Loop System

The mapping describing the system behavior between the time instants kT and $(k+1)T$ can be obtained by composing the two previously presented local mappings [2], i.e., the Poincaré map $P = P_2 \circ P_1$ of the switched PWM system described by the vector fields given in (1) and (2) can be written in the following form

$$\mathbf{x}_{k+1} = \boldsymbol{\Phi}(d_k)\mathbf{x}_k + \boldsymbol{\Psi}(d_k) \tag{7}$$

where $\boldsymbol{\Phi}(d_k)$ and $\boldsymbol{\Psi}(d_k)$ are given by:

$$\boldsymbol{\Phi}(d_k) := \boldsymbol{\Phi}_2((1-d_k)T)\boldsymbol{\Phi}_1(d_kT) \tag{8a}$$

$$\boldsymbol{\Psi}(d_k) := \boldsymbol{\Phi}_2((1-d_k)T)\boldsymbol{\Psi}_1(d_kT) + \boldsymbol{\Psi}_2(d_kT) \tag{8b}$$

3.4 Closing the Loop: The Source of Nonlinearity

For appropriate operation of PWM systems and regulation of some suitable outputs in the presence of parameter changes, output feedback is used. Often an integrative action is necessary in order to regulate a certain output variable x_o to get a zero steady-state error between this output variable and the desired reference x_{ref}. First, the error $e := x_{\text{ref}} - x_o$ is computed and then it is processed through a compensator containing an integrator to increase, in average, the DC gain of the system while other poles and zeroes of the compensator are selected with the aim to meet some design specifications like maximum allowed overshoot and system response speed and settling time due to step changes. As it has been mentioned before, this integral action has a negligible effect on the fast scale instability [6]. Therefore, we exclude the integral variable from the analysis. The feedback loop together with the PWM process imposes the following constraint between the state variables $\mathbf{x}(d_kT)$ and the duty cycle d_k at the kth switching cycle

$$\begin{aligned}\sigma(\mathbf{x}(d_kT), d_k) :&= -\mathbf{C}^{\intercal}\mathbf{x}_d - r(d_kT) \\ &= -\mathbf{C}^{\intercal}\boldsymbol{\Phi}_1(d_kT)\mathbf{x}_k + \boldsymbol{\Psi}_1(d_kT) - r(d_kT) = 0\end{aligned} \tag{9}$$

The expression in (9) is nonlinear in d_k and it is responsible for many nonlinear phenomena that could take place in PWM systems.

3.5 Steady-State Response of the Poincaré Map

In this section, let D be the steady-state duty cycle. Let also $\boldsymbol{\Phi}_1 = e^{\mathbf{A}_1 DT}$ and $\boldsymbol{\Phi}_2 = e^{\mathbf{A}_2(1-D)T}$, $\boldsymbol{\Psi}_1 = \mathbf{A}_1^{-1}(e^{\mathbf{A}_i DT} - \mathbf{I})\mathbf{B}_1\mathbf{w}$ and $\boldsymbol{\Psi}_2 = \mathbf{A}_2^{-1}(e^{\mathbf{A}_i((1-D)T)} - \mathbf{I})\mathbf{B}_2\mathbf{w}$. Let $\mathbf{x}_{ss}(0)$ be the steady-state value of the periodic orbit of the system at the beginning

of the switching period and $\mathbf{x}_{ss}(DT)$ be the steady-state value of this orbit at time instant DT. Therefore, in steady-state, according to (4), the vector of state variables at the beginning of the switching period is given by (Fig. 1)

$$\mathbf{x}_{ss}(0) = \mathbf{x}_{ss}(T) = \mathbf{\Phi}_2 \mathbf{x}_{ss}(DT) + \mathbf{\Psi}_2 \tag{10}$$

In turn, the vector of state variables at the switching time DT within the same period can be expressed as follows

$$\mathbf{x}_{ss}(DT) = \mathbf{\Phi}_1 \mathbf{x}_{ss}(0) + \mathbf{\Psi}_1 \tag{11}$$

Using (10) in (11), one obtains

$$\mathbf{x}_{ss}(DT) = \mathbf{\Phi}_1 \mathbf{\Phi}_2 \mathbf{x}_{ss}(DT) + \mathbf{\Phi}_1 \mathbf{\Psi}_2 + \mathbf{\Psi}_1 \tag{12}$$

Therefore, the steady-state value of the state variables $\mathbf{x}_{ss}(DT)$ at the time instant DT is given by

$$\mathbf{x}_{ss}(DT) = (\mathbf{I} - \mathbf{\Phi}_1 \mathbf{\Phi}_2)^{-1} (\mathbf{\Phi}_1 \mathbf{\Psi}_2 + \mathbf{\Psi}_1) \tag{13}$$

Let $\mathbf{\Phi} = \mathbf{\Phi}_1 \mathbf{\Phi}_2$ and $\mathbf{\Psi} = \mathbf{\Phi}_1 \mathbf{\Psi}_2 + \mathbf{\Psi}_1$. Then, (13) can be simplified as follows

$$\mathbf{x}_{ss}(DT) = (\mathbf{I} - \mathbf{\Phi})^{-1} \mathbf{\Psi} \tag{14}$$

where the matrix $(\mathbf{I} - \mathbf{\Phi})$ is assumed to be nonsingular. It should be noted that the previous system is open loop stable if the integral state variable is excluded because the matrices $\mathbf{A}_i$ are supposed to represent dissipative linear system configuration. The monodromy matrix of the open loop system is the product of the monodromy matrices corresponding to the two linear configurations. Both monodromy matrices are stable because they are exponential matrix functions of Hurwitz matrices. Therefore, the product of both monodromy matrices is a Jury matrix and then the open loop system is stable. Note also that if the integrator was included in the model, the open loop system response would be unbounded unless the input to the integrator is zero.

The stability of periodic orbits of a closed loop PWM system can be analyzed by checking the evolution of a small perturbation in the state variable within one period. This problem can be tackled by different ways. One of the most used techniques is to analyze the stability of the fixed points of the Poincaré map of the closed loop system by using its Jacobian matrix. The periodic orbit will be stable if this matrix evaluated at the associated fixed point has eigenvalues with modulus less than 1. Another technique is by using Floquet theory and Filippov method which leads to the same results [6]. In this chapter a different approach will be used which is based on the analysis of the steady-state response of the Poincaré map to periodic and subharmonic excitations [26].

4 A Steady-State Approach for Predicting Fast Time-Scale Instabilities

Using the steady-state response for predicting fast-scale instability in the form of subharmonic oscillation has been first introduced in [17] for a simple case of a PWM system with linear plant which consists of a DC-DC buck converter under voltage mode control. Years later, this method has been re-considered in [3, 5]. The method in both works consists of a Fourier series expansion of the feedback signal and its use for predicting stability boundaries after imposing a certain system periodic regime by the PWM process. With that approach an effort to transform the results from the Fourier frequency-domain into the time-domain must be done. In [5], the transformation from the Fourier frequency-domain to the time-domain is based on elementary partial fraction decomposition after defining some elementary cases of the system *transfer function* in the $s-$domain and listing them in the form of tables. However, this transfer function cannot be directly defined for systems with $\mathbf{A}_2 \neq \mathbf{A}_1$ making the approach only applicable for a limited class of PWM systems like the ones considered in [5]. In particular, those can be formulated in the form of a linear subsystem and a square-wave signal generated by a comparator like the PWM process. It should be noted that in [5] the approach is based on the Fourier series expansion to a system with theoretically $\mathbf{A}_2 \neq \mathbf{A}_1$ was applied but by making an approximation and an order reduction leading finally to the simple linear case $\mathbf{A}_1 = \mathbf{A}_2$. Another different type of approximation leading to the same consequence $\mathbf{A}_1 = \mathbf{A}_2$ has been used and justified in [7] for this kind of systems. In [20], the Poisson sum formulae and some related Fourier series properties have been used to transform the condition for PD occurrence derived in [5] from the Fourier frequency-domain to a matrix-form state-space time-domain condition. It was shown in this study that a steady-state analysis of the trajectory of the system in the time-domain without any order reduction, except from excluding the integrator, will lead to new equivalent simple expressions without need to use the Fourier series expansion and without having to perform any transformation nor needing the calculation of the Jacobian or the monodromy matrix.

4.1 Predicting SN Bifurcation

SN bifurcation or *tangent* bifurcation is a type of local bifurcations that can take place in nonlinear continuous-time dynamical systems. This nonlinear phenomenon is characterized by the fact that two solutions of a continuous system collide and annihilate each other at a certain critical value of the system bifurcation parameter. When the system is represented by a Poincaré mapping obtained by sampling a continuous-time system as it is the case in PWM systems, these solutions correspond to periodic orbits of the original system and the phenomenon is also called *cyclic fold* bifurcation.

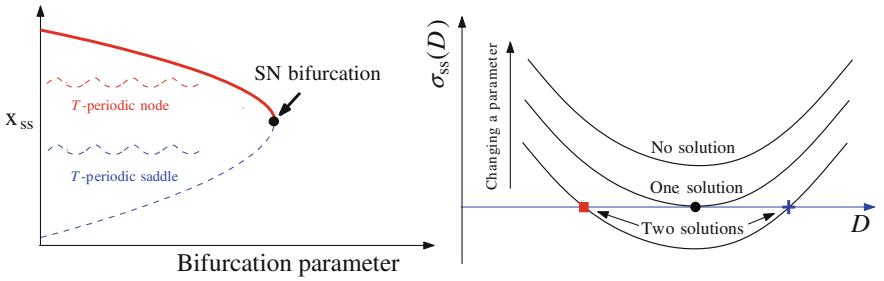

Fig. 3 SN bifurcation in a nonlinear dynamical system

In steady state the feedback loop together with the PWM process imposes the following constraint between the state variables $\mathbf{x}_{ss}(DT)$ and the steady-state duty cycle D

$$\sigma_{ss}(D) := \sigma(\mathbf{x}_{ss}(DT), DT) := -\mathbf{C}^{\intercal}\mathbf{x}_{ss}(DT) - r(DT) = 0 \tag{15}$$

If a SN bifurcation takes place at a certain critical value of the system bifurcation parameter, there must be a tangency between the feedback signal—$\mathbf{C}^{\intercal}x_{ss}(DT)$ and the ramp signal $r(DT)$ for the imposed steady-state duty cycle D in such a way that two solutions of (15) coalesce and disappear (Fig. 3). The number of solutions of (15) equals to the number of T—periodic orbits that exist for a specific set of parameters. Therefore, from (15), the following equality holds at this critical point

$$\frac{\partial \sigma_{ss}(D)}{\partial D} = 0 \Rightarrow -\frac{\partial \mathbf{C}^{\intercal}\mathbf{x}_{ss}(DT)}{\partial D} = \frac{\partial r(DT)}{\partial D} \tag{16}$$

Let $\sigma_e(D) = 1/T \times \partial r/\partial D$ be the slope of the external T—periodic signal $r(t)$ at time instant DT. Therefore, (16) becomes

$$-\frac{1}{T}\mathbf{C}^{\intercal}\frac{\partial \mathbf{x}_{ss}(DT)}{\partial D} = \sigma_e(D) \tag{17}$$

The derivative of the left side of (17) can be obtained by using (14) and differentiating the involved matrix functions. Let us calculate the derivative $\partial \mathbf{x}_{ss}(DT)/\partial D$. Using (14) one obtains

$$\frac{\partial \mathbf{x}_{ss}(DT)}{\partial D} = \frac{\partial}{\partial D}(\mathbf{I} - \mathbf{\Phi})^{-1}\mathbf{\Psi} + (\mathbf{I} - \mathbf{\Phi})^{-1}\frac{\partial \mathbf{\Psi}}{\partial D} \tag{18}$$

Using known chain rules for matrix derivative, (18) can be written as follows

$$\frac{\partial \mathbf{x}_{ss}(DT)}{\partial T} = (\mathbf{I} - \mathbf{\Phi})^{-1}\frac{\partial \mathbf{\Phi}}{\partial D}(\mathbf{I} - \mathbf{\Phi})^{-1}\mathbf{\Psi} + (\mathbf{I} - \mathbf{\Phi})^{-1}\frac{\partial \mathbf{\Psi}}{\partial D} \tag{19}$$

Making the term $(\mathbf{I}-\mathbf{\Phi})^{-1}$ as a common factor results in the following equation

$$\frac{\partial \mathbf{x}_{\mathrm{ss}}(DT)}{\partial D} = (\mathbf{I}-\mathbf{\Phi})^{-1}\left(\frac{\partial \mathbf{\Phi}}{\partial D}(\mathbf{I}-\mathbf{\Phi})^{-1}\mathbf{\Psi} + \frac{\partial \mathbf{\Psi}}{\partial D}\right) \tag{20}$$

then by using (14), the expression (20) becomes

$$\frac{\partial \mathbf{x}_{\mathrm{ss}}(DT)}{\partial D} = (\mathbf{I}-\mathbf{\Phi})^{-1}\left(\frac{\partial \mathbf{\Phi}}{\partial D}\mathbf{x}(DT) + \frac{\partial \mathbf{\Psi}}{\partial D}\right) \tag{21}$$

The derivative of the involved matrix function $\partial\mathbf{\Phi}(D)/\partial D$ can be calculated as follows

$$\begin{aligned}\frac{\partial \mathbf{\Phi}}{\partial D} &= \frac{\partial}{\partial D}(\mathbf{\Phi}_1\mathbf{\Phi}_2)\\ &= \mathbf{\Phi}_1(\mathbf{A}_1-\mathbf{A}_2)\mathbf{\Phi}_2 T\end{aligned} \tag{22}$$

Likewise, the derivative of $\partial\mathbf{\Psi}(D)/\partial D$ can be obtained by

$$\begin{aligned}\frac{\partial \mathbf{\Psi}}{\partial D} &= \frac{\partial}{\partial D}(\mathbf{\Phi}_1\mathbf{\Psi}_2+\mathbf{\Psi}_1)\\ &= \frac{\partial}{\partial D}(\mathbf{\Phi}_1)\mathbf{\Psi}_2 + \mathbf{\Phi}_1\frac{\partial}{\partial D}(\mathbf{\Psi}_2) + \frac{\partial}{\partial D}(\mathbf{\Psi}_1)\\ &= \mathbf{\Phi}_1((\mathbf{A}_1-\mathbf{A}_2)\mathbf{\Psi}_2 + \mathbf{B}_1-\mathbf{B}_2)T\end{aligned} \tag{23}$$

Let $\Delta\mathbf{A} = \mathbf{A}_1-\mathbf{A}_2$ and $\Delta\mathbf{B} = \mathbf{B}_1-\mathbf{B}_2$. Substituting (22) and (23) in (21), the critical boundary condition for SN bifurcation boundary in (17) becomes

$$\sigma_{e,\mathrm{SN}}(D) = \sigma_e(D) \tag{24}$$

where $\sigma_{e,\mathrm{SN}}(D)$, the critical slope of the external function $r(t)$ for SN bifurcation occurrence, can be expressed by

$$\sigma_{e,\mathrm{SN}}(D) = -\mathbf{C}^{\intercal}(\mathbf{I}-\mathbf{\Phi})^{-1}\mathbf{\Phi}_1(\Delta\mathbf{A}\mathbf{x}_{ss}(0)+\Delta\mathbf{B}) \tag{25}$$

Taking into account that $\mathbf{A}_1\mathbf{x}(t)+\mathbf{B}_1 = \dot{\mathbf{x}}(t^-) = \mathbf{f}_1(\mathbf{x},\mathbf{w})$ and that $\mathbf{A}_2\mathbf{x}(t)+\mathbf{B}_2 = \dot{\mathbf{x}}(t^+) = \mathbf{f}_2(\mathbf{x},\mathbf{w})$, the critical value of the slope of the external T—periodic function at the boundary of a SN bifurcation is

$$\sigma_{e,\mathrm{SN}}(D) = -\mathbf{C}^{\intercal}(\mathbf{I}-\mathbf{\Phi})^{-1}\mathbf{\Phi}_1\Delta\mathbf{f}(\mathbf{x}_{\mathrm{ss}}(0)) \tag{26}$$

where $\Delta\mathbf{f}(\mathbf{x}) = \mathbf{f}_1(\mathbf{x},\mathbf{w}) - \mathbf{f}_2(\mathbf{x},\mathbf{w})$. It has to be mentioned here that in [4, 8] a slightly differently expressed condition has been obtained for the same boundary condition which is reported and adapted here for comparison

$$\sigma_{e,\mathrm{SN}}(D) = -\mathbf{C}^{\mathsf{T}}[\mathbf{f}_1(\mathbf{x}_{\mathrm{ss}}(D^-T)) + \mathbf{\Phi}_1(\mathbf{I} - \mathbf{\Phi}_2\mathbf{\Phi}_1)^{-1}])\mathbf{\Phi}_2\Delta\mathbf{f}(\mathbf{x}_{\mathrm{ss}}(DT)) \quad (27)$$

Although apparently the condition (27) derived in [4, 8] and that in (26) do not coincide, they just happen to be the same conditions but expressed differently. Note however that the expression (26) is simpler than (27). To illustrate the use of the previous expression, let us consider the following three different cases of compensating external signals:

- Case of a linear compensating ramp signal

$$r(t) = r_0 + \sigma_e t \quad (28)$$

where r_0 is the initial value of the external signal at $t = 0$ and σ_e is its constant slope. This is the ideal case of most PWM systems. Since the slope is constant, the right-hand side of (24) is given by

$$\sigma_e(D) = \sigma_e \ \forall D \quad (29)$$

- Case of a quadratic modulating signal. For improving the performances of some switching PWM systems, a quadratic modulating signal can be used [21, 22]. Let σ_0 be the initial slope of the external signal at $t = 0$ and let σ_T be its final slope at $t = T$. Therefore, this signal can be expressed as follows

$$r(t) = r_0 + \sigma_0 t + \frac{1}{2T}(\sigma_T - \sigma_0)t^2 \quad (30)$$

In this case, the slope is linearly dependent on the duty cycle D and the right-hand side of (24) can be expressed as follows

$$\sigma_e(D) = \sigma_0 + (\sigma_T - \sigma_0)D \quad (31)$$

- In a practical implementation, the external modulating signal is implemented by a first order low pass filter system making its shape more exponential than linear. In this case, the ramp signal $r(t)$ can be expressed as follows

$$r(t) = r_0 + \sigma_0\tau(1 - e^{-\frac{t}{\tau}}) \quad (32)$$

where τ is a suitable time constant and σ_0 is the initial slope at the beginning of the switching cycle. The slope is exponentially depending on the duty cycle D and the right-hand side of (24) is given by

$$\sigma_e(D) = \sigma_0 e^{-\frac{DT}{\tau}} \quad (33)$$

4.2 Application Examples for Predicting SN Bifurcation

4.2.1 General Bilinear Plants

Example 1: Consider a boost converter under state feedback control with the parameter values considered in [23] (Fig. 4). These are: input voltage $v_g = 5$ V, inductance $L = 50$ μH, capacitance $C = 4.4$ μF, voltage feedback gain $k_v = -0.0435$, current feedback gain $k_i = 0.174$ Ω, voltage reference $V_{\text{ref}} = 0.13$ V, load resistance $R = 28$ Ω. Three different values of switching frequency are used to illustrate the occurrence of SN bifurcation. The system matrices and vectors are as follows

$$\mathbf{A}_1 = \begin{pmatrix} -\frac{1}{RC} & 0 \\ 0 & 0 \end{pmatrix}, \mathbf{A}_2 = \begin{pmatrix} -\frac{1}{RC} & \frac{1}{C} \\ -\frac{1}{L} & 0 \end{pmatrix}$$

$$\mathbf{B}_1 = \mathbf{B}_2 = \begin{pmatrix} 0 \\ \frac{1}{L} \end{pmatrix}, \quad \mathbf{x} = \begin{pmatrix} v_{C_1} \\ i_{L1} \end{pmatrix}, \quad \mathbf{w} = v_g, \quad \mathbf{C} = \begin{pmatrix} k_v \\ k_i \end{pmatrix}$$

All the parameters appearing in the matrices can be identified in the circuit diagram of Fig. 4.

Numerical simulations in [23] confirm that the system is stable for switching frequencies greater than $f_s = 500$ kHz and unstable for lower frequencies. For f_s =500 kHz, it was shown in [24] that the system has one stable operating solution with duty

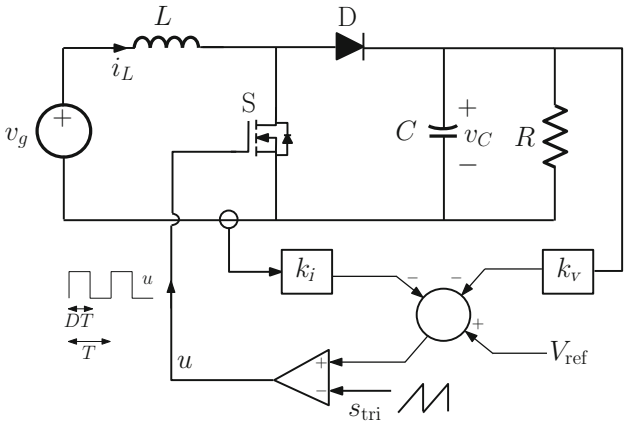

Fig. 4 Boost converter under a state feedback control

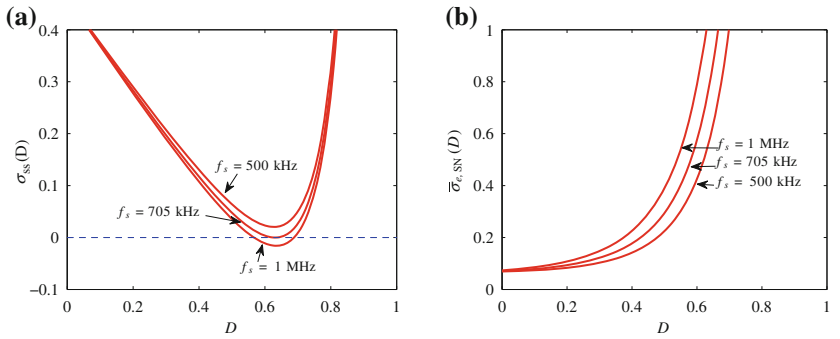

Fig. 5 The switching function $\sigma_{ss}(D)$ showing the disappearance of two solutions near a SN bifurcation (**a**) and the stability map in terms of the duty cycle and the normalized slope ($\overline{\sigma}_e = \sigma_e/(v_g/L)$) of the signal r (**b**)

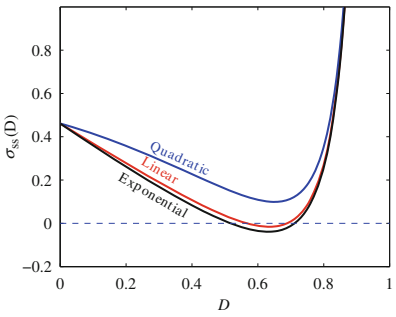

Fig. 6 The effect of the type of the modulator on the SN bifurcation

cycles $D \approx 0.58$ and one unstable solution with $D \approx 0.70$. This instability has been explained numerically by expanding the system waveforms in the form of a Fourier series and a Picard iterative process applied to the function $f(D) = -\mathbf{C}^{\mathrm{T}}\mathbf{x}(DT)$. The statement in [23] that the system is unstable has been refined using the concept of the basin of attraction. It has been stated that starting in the (possibly small) basin of attraction of the behavior corresponding to the stationary duty cycle $D \approx 0.58$ the system converges to a periodic regime characterized by this duty cycle value. Hence, starting in this domain of attraction the system exhibits a stable behavior. However, transient solutions outside this basin are unstable and the system do not converge to the desired periodic regime. Here we confirm the result reported in [24] by using the new derived expression (26) and we show that the critical value for occurrence of SN bifurcation is $f_s \approx 705$ kHz.

Figure 5a shows the boundary of SN in the parameter space (D, σ_e) by considering a linear ramp modulator for different values of switching frequency f_s. Figure 5b shows the steady-state switching function $\sigma_{ss}(D)$ for the same values of the switching frequency where it can be observed that for $f_s \approx 705$ kHz the system is indeed at the boundary of SN bifurcation. In order to show the effect of the type of the modulator signal on the system behavior, Fig. 6 shows the switching function $\sigma_{ss}(D)$ in term

of the steady-sate duty cycle D. The switching frequency is fixed at $f_s = 1$ MHz. It can be observed that while the stability is improved with an exponential modulator, it is worsened in the case of a quadratic modulator. For a fair comparison, the same value of ramp amplitude $V_M = 1$ V is used for the three modulators.

4.2.2 Special Linear Plants

Example 2: The second example that will be considered in this study is a buck converter driving another converter both under current mode control. The second converter can be approximated by a constant current sink [25]. All the parameters appearing in the matrices can be identified in the circuit diagram of Fig. 7. Because $\mathbf{A}_1 = \mathbf{A}_2$, the plant is linear. The used parameter values are the same ones of [25] and are as follows: input voltage $v_g = 120$ V, inductance $L = 37.5\,\mu$H, DC parasitic of the inductance $r_L = 0.01\ \Omega$, capacitance value $C = 420\,\mu$F, equivalent series resistance of the capacitor $r_C = 0.01\ \Omega$, output current $i_o = 38$ A and switching frequency $f_s = 50$ kHz. The system matrices and vectors are as follows

$$\mathbf{A}_1 = \mathbf{A}_2 = \begin{pmatrix} 0 & \frac{1}{C} \\ -\frac{1}{L} & -\frac{r_L + r_C}{L} \end{pmatrix},$$

$$\mathbf{B}_1 = \begin{pmatrix} \frac{1}{C} & 0 \\ \frac{1}{L} & \frac{r_C}{L} \end{pmatrix}, \quad \mathbf{B}_2 = \begin{pmatrix} \frac{1}{C} & 0 \\ 0 & \frac{r_C}{L} \end{pmatrix},$$

$$\mathbf{x} = \begin{pmatrix} v_C \\ i_L \end{pmatrix}, \quad \mathbf{w} = \begin{pmatrix} v_g \\ i_o \end{pmatrix}, \quad \mathbf{C_1} = \begin{pmatrix} 1 \\ 0 \end{pmatrix}$$

Figure 8 shows $\sigma_{\text{ss}}(D)$ which gives the possible operating steady-state duty cycles for different values of i_{ref} just below and just above the SN critical point. This figure also shows the stability map of the system in the parameter space (D, σ_e). For $D < 0.5$, the system has only one solution. For $D > 0.5$, three different regions can be identified. The first one is $\sigma_e < \sigma_{e,\text{SN}}$ where the system presents no solution. The second one is $\sigma_{e,\text{SN}} < \sigma_e < V_g/(2L)$ where the system presents one stable solution and one saddle. The last one where $\sigma_e > V_g/(2L)$ and the system presents one stable solution. For this particular example it turns out that the boundary of the SN bifurcation in the parameter space (D, σ_e) is approximately a straight line whose slope is V_g/L and passing from $D = 0.5$ and its maximum value is $V_g/(2L)$ for $D = 1$. Therefore, by choosing $\sigma_e = V_g/(2L)$ will guarantee that the system to have only one solution independently on the value of the steady-state cycle.

4.3 A Steady-State Approach for Predicting PD Bifurcation

4.3.1 Steady-State Response of the Second Iterate Poincaré Map

Consider a switched dynamical system under PWM exhibiting a PD bifurcation as shown in Fig. 9. After this phenomenon takes place, a $2T$-periodic solution develops at the critical point while in contrast to the SN bifurcation case, the T-periodic solution loses its stability but it continues to exist. During the switching cycle of duration T, a PWM system has two phases defined by the system matrices $(\mathbf{A}_1, \mathbf{B}_1)$ and $(\mathbf{A}_2, \mathbf{B}_2)$, respectively. During the switching cycle of duration $2T$, this system has four phases defined by the system matrices $(\mathbf{A}_1, \mathbf{B}_1)$, $(\mathbf{A}_2, \mathbf{B}_2)$, $(\mathbf{A}_1, \mathbf{B}_1)$ and $(\mathbf{A}_2, \mathbf{B}_2)$, respectively. Let us assume that the system behavior in steady-state is a $2T$-periodic orbit. Therefore, during two consecutive switching periods in the interval $(kT, (k+2)T)$, let the crossing between the signals $-\mathbf{C}^\intercal\mathbf{x}(t)$ and $r(t)$ occurs at $t = (D - \varepsilon_t + k)T$ and at $t = (1 + D + \varepsilon_t + k)T$, $k \in \mathbb{Z}$ (see Fig. 10). The parameter ε_t is a small quantity that vanishes at the boundary between T—periodic and $2T$-periodic behavior. At this point, the T-periodic solution and the $2T$-periodic solution are coincident (Fig. 9). By obtaining the expression of the $2T$-periodic steady-state solutions at the switching instants, imposing the corresponding feedback constraints imposed by the PWM process and equating them at the critical point ($\varepsilon_t \to 0$), a condition for predicting PD bifurcation is obtained in terms of the system matrices containing all the parameters.

From the switching conditions at the two switching instants $t = (D + \varepsilon_t)T$ and $t = (1 + D + \varepsilon_t)T$, the following equalities hold

$$-\mathbf{C}^\intercal\mathbf{x}_{ss}((D - \varepsilon_t)T) = r((D - \varepsilon_t)T) \tag{34a}$$

$$-\mathbf{C}^\intercal\mathbf{x}_{ss}((D + \varepsilon_t + 1)T) = r((D + \varepsilon_t)T) \tag{34b}$$

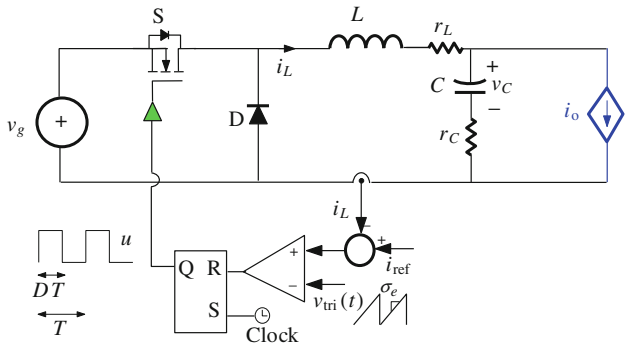

Fig. 7 Schematic circuit diagram of a buck converter under a current mode control loaded by a constant current source as a load representing a downstream converter also under current mode control

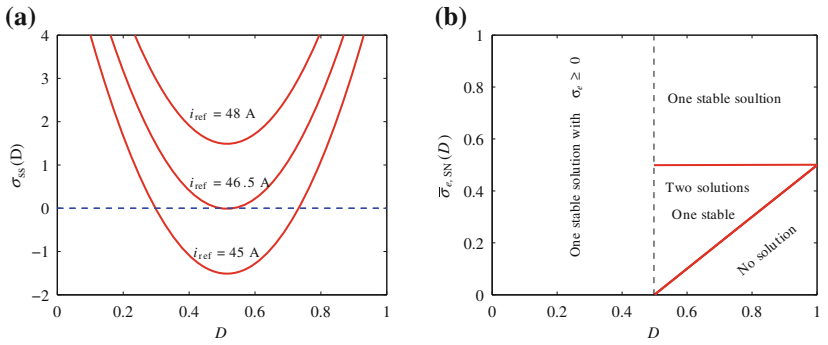

Fig. 8 The switching function $\sigma_{ss}(D)$showing the disappearance of two solutions near a SN bifurcation (**a**) and the stability map in terms of the duty cycle and the slope of the signal r (**b**)

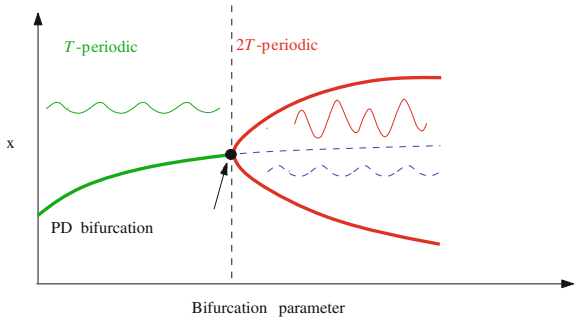

Fig. 9 Sketch of a PD bifurcation in a switched dynamical system under PWM and the corresponding waveforms before and after the bifurcation takes place by sweeping a parameter

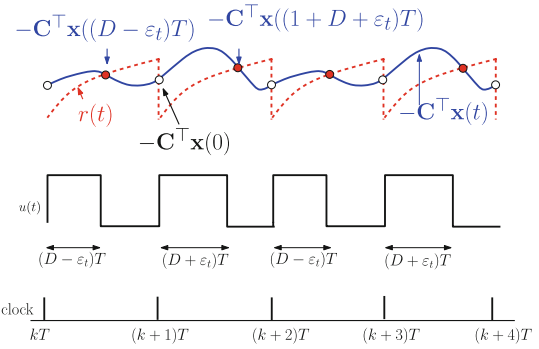

Fig. 10 Waveforms of the T—periodic external signal $r(t)$ and the feedback signal $-\mathbf{C}^\top\mathbf{x}_{ss}(t)$ at $2T$—periodic regime in steady-state

While in [5], the previous equations are expressed in the Fourier frequency domain in the case of an example of PWM systems with linear plant for which $\mathbf{A}_1 = \mathbf{A}_2$, in this chapter these two equations are treated generally for the bilinear case directly in the time-domain without any extra effort to go back from the Fourier frequency-domain into the time-domain. Exhibiting a $2T$-periodic regime, the sampled value of the steady-state variables of the system at the switching instants $(D - \varepsilon_t)T$ and

$(D+\varepsilon_t+1)T$ can be obtained by using (4) and forcing $2T$—periodicity. By doing so, it can be expressed as follows

$$\mathbf{x}_{ss}((D-\varepsilon_t)T) = (\mathbf{I}-\boldsymbol{\Phi}_-(\varepsilon_t))^{-1}\boldsymbol{\Psi}_-(\varepsilon_t) \tag{35a}$$

$$\mathbf{x}_{ss}((D+\varepsilon_t+1)T) = (\mathbf{I}-\boldsymbol{\Phi}_+(\varepsilon_t))^{-1}\boldsymbol{\Psi}_+(\varepsilon_t) \tag{35b}$$

where all the matrices and vectors appearing in the previous equations are given by

$$\boldsymbol{\Phi}_-(\varepsilon_t) = \bar{\boldsymbol{\Phi}}_1\bar{\boldsymbol{\Phi}}_4\bar{\boldsymbol{\Phi}}_3\bar{\boldsymbol{\Phi}}_2 \tag{36a}$$

$$\boldsymbol{\Phi}_+(\varepsilon_t) = \bar{\boldsymbol{\Phi}}_3\bar{\boldsymbol{\Phi}}_2\bar{\boldsymbol{\Phi}}_1\bar{\boldsymbol{\Phi}}_4 \tag{36b}$$

$$\boldsymbol{\Psi}_-(\varepsilon_t) = \bar{\boldsymbol{\Phi}}_1\bar{\boldsymbol{\Phi}}_4\bar{\boldsymbol{\Phi}}_3\bar{\boldsymbol{\Psi}}_2 + \bar{\boldsymbol{\Phi}}_1\bar{\boldsymbol{\Phi}}_4\bar{\boldsymbol{\Psi}}_3 + \bar{\boldsymbol{\Phi}}_1\bar{\boldsymbol{\Psi}}_4 + \bar{\boldsymbol{\Psi}}_1 \tag{36c}$$

$$\boldsymbol{\Psi}_+(\varepsilon_t) = \bar{\boldsymbol{\Phi}}_3\bar{\boldsymbol{\Phi}}_2\bar{\boldsymbol{\Phi}}_1\bar{\boldsymbol{\Psi}}_4 + \bar{\boldsymbol{\Phi}}_3\bar{\boldsymbol{\Phi}}_2\bar{\boldsymbol{\Psi}}_1 + \bar{\boldsymbol{\Phi}}_3\bar{\boldsymbol{\Psi}}_2 + \bar{\boldsymbol{\Psi}}_3 \tag{36d}$$

and

$$\bar{\boldsymbol{\Phi}}_1 = \boldsymbol{\Phi}_1 e^{-\mathbf{A}_1\varepsilon_t T},\quad \bar{\boldsymbol{\Psi}}_1 = \int_0^{(D-\varepsilon_t)T} e^{\mathbf{A}_1\tau}\mathrm{d}\tau\mathbf{B}_1\mathbf{w} \tag{37a}$$

$$\bar{\boldsymbol{\Phi}}_2 = \boldsymbol{\Phi}_2 e^{\mathbf{A}_2\varepsilon_t T},\quad \bar{\boldsymbol{\Psi}}_2 = \int_0^{(1-D+\varepsilon_t)T} e^{\mathbf{A}_2\tau}\mathrm{d}\tau\mathbf{B}_2\mathbf{w} \tag{37b}$$

$$\bar{\boldsymbol{\Phi}}_3 = \boldsymbol{\Phi}_1 e^{\mathbf{A}_1\varepsilon_t T},\quad \bar{\boldsymbol{\Psi}}_3 = \int_0^{(D+\varepsilon_t)T} e^{\mathbf{A}_1\tau}\mathrm{d}\tau\mathbf{B}_1\mathbf{w} \tag{37c}$$

$$\bar{\boldsymbol{\Phi}}_4 = \boldsymbol{\Phi}_2 e^{-\mathbf{A}_2\varepsilon_t T},\quad \bar{\boldsymbol{\Psi}}_4 = \int_0^{(1-D-\varepsilon_t)T} e^{\mathbf{A}_2\tau}\mathrm{d}\tau\mathbf{B}_2\mathbf{w} \tag{37d}$$

Subtracting (34a) from (34b), one obtains

$$-\mathbf{C}^{\mathsf{T}}(\mathbf{x}_{ss}((D+1+\varepsilon_t)T)-\mathbf{x}_{ss}((D-\varepsilon_t)T)) = r((D+\varepsilon_t)T)-r((D-\varepsilon_t)T) \tag{38}$$

The boundary of PD bifurcation can be located by taking the limit in (38) when the parameter $\varepsilon_t \to 0$. Therefore, at the onset of this instability the following equality holds

$$-\lim_{\varepsilon_t\to 0}\mathbf{C}^{\mathsf{T}}(\mathbf{x}_{ss}((D+1+\varepsilon_t)T)-\mathbf{x}_{ss}((D-\varepsilon_t)T)) = \lim_{\varepsilon_t\to 0} r((D+\varepsilon_t)T)-r((D-\varepsilon_t)T) \tag{39}$$

While the right-hand side of (39) is generally easy to obtain, the left-hand side of the previous equation is mathematically more involved. Let us first focus on the right-hand side of (39) and let us obtain it for three different cases of PWM signals:

- In the case of a linear ramp compensating signal, the right-hand side of (39) is given by

$$\lim_{\varepsilon_t \to 0} r((D+\varepsilon_t)T) - r((D-\varepsilon_t)T) = 2\sigma_e T \tag{40}$$

- In the case of a quadratic modulating signal, the right-hand side of (39) can be easily expressed as follows

$$\lim_{\varepsilon_t \to 0} r((D+\varepsilon_t)T) - r((D-\varepsilon_t)T) = 2T(\sigma_0 + (\sigma_T - \sigma_0)D) \tag{41}$$

- In a practical implementation, the slope is exponentially depending on the duty cycle D and the right-hand side of (39) is given by

$$\lim_{\varepsilon_t \to 0} r((D+\varepsilon_t)T) - r((D-\varepsilon_t)T) = 2\sigma_0 T e^{-\frac{DT}{\tau}} \tag{42}$$

As it was mentioned previously, the left-hand side of the previous equation is mathematically more involved. For simplicity let us consider that the external T—periodic function is linear during the switching period in such a way that its slope σ_e is constant and that (39) can be written as follows

$$\sigma_{e,\mathrm{PD}}(D) = \sigma_e \tag{43}$$

where $\sigma_{e,\mathrm{PD}}(D)$, the critical slope for PD bifurcation boundary, is given by

$$\sigma_{e,\mathrm{PD}}(D) = -\lim_{\varepsilon_t \to 0} \frac{1}{2\varepsilon_t T} \mathbf{C}^{\intercal}(\mathbf{x}_{ss}((D+1+\varepsilon_t)T) - \mathbf{x}_{ss}((D-\varepsilon_t)T)) \tag{44}$$

By using (35a)–(35b), the limit expression in (44) becomes

$$\sigma_{e,\mathrm{PD}}(D) = -\lim_{\varepsilon_t \to 0} \frac{1}{2\varepsilon_t T}((\mathbf{I} - \Phi_+(\varepsilon_t))^{-1}\boldsymbol{\Psi}_+(\varepsilon_t) - (\mathbf{I} - \boldsymbol{\Phi}_-(\varepsilon_t))^{-1}\boldsymbol{\Psi}_-(\varepsilon_t)) \tag{45}$$

By calculating the limit in the previous expression, the following condition is obtained at the boundary of subharmonic oscillation

$$\sigma_{e,\mathrm{PD}}(D) = -\mathbf{C}^{\intercal}[(\mathbf{I} - \boldsymbol{\Phi})^{-1}\boldsymbol{\Phi}_1(\mathbf{f}_1(\mathbf{x}_{\mathrm{ss}}(0)) + \mathbf{f}_2(\mathbf{x}_{\mathrm{ss}}(0)))] \tag{46}$$

More calculation details can be found in [26]. It is worth mentioning here that in [4], a slightly differently expressed condition has been obtained using a different approach based on solving the eigenvalue problem of the z-domain characteristic equation, for the same boundary condition which is reported and adapted here for comparison

$$\sigma_{e,\mathrm{PD}}(D) = -\mathbf{C}^{\mathsf{T}}[\mathbf{f}_1(\mathbf{x}_{\mathrm{ss}}(DT^-)) - \boldsymbol{\Phi}_1(\mathbf{I} - \boldsymbol{\Phi}_2\boldsymbol{\Phi}_1)^{-1}]\boldsymbol{\Phi}_2\Delta\mathbf{f}(\mathbf{x}_{\mathrm{ss}}(DT)) \quad (47)$$

Although they are expressed differently, the critical ramp slope for PD bifurcation given in (46) and the one derived in [4] and shown in (47), are coincident. Note however that (46) is simpler than (47).

4.4 Application Examples for Predicting PD Bifurcation

4.4.1 General Bilinear Plants

Example 3: The system which will be considered in this section is a boost converter under a current mode peak controller. The state variables are the capacitor voltage v_C and the inductor current i_L. The system matrices and vectors are as follows

$$\mathbf{A}_1 = \begin{pmatrix} -\frac{1}{RC} & 0 \\ 0 & -\frac{r_L}{C} \end{pmatrix}, \quad \mathbf{A}_2 = \begin{pmatrix} -\frac{1}{RC} & \frac{1}{C} \\ \frac{1}{C} & -\frac{r_L}{C} \end{pmatrix}$$

$$\mathbf{B}_1 = \mathbf{B}_2 = \begin{pmatrix} 0 \\ \frac{1}{L} \end{pmatrix}, \quad \mathbf{x} = \begin{pmatrix} v_C \\ i_L \end{pmatrix}, \quad \mathbf{w} = v_g, \quad \mathbf{C} = \begin{pmatrix} 0 \\ 1 \end{pmatrix}$$

where R is the load resistance, L is the inductance with equivalent series resistance r_L, C is the output filtering capacitance and v_g is the input voltage. The peak current is i_{ref}. The duty cycle D is varied by varying i_{ref}. The used parameter values are as follows: input voltage $v_g = 5\,\mathrm{V}$, inductance $L = 200$ $\mu\mathrm{H}$, DC parasitic of the inductance $r_L = 0.1\ \Omega$, capacitance value $C = 10\,\mu\mathrm{F}$, load resistance $R = 15\ \Omega$ and switching frequency $f_s = 10\,\mathrm{kHz}$.

It can be demonstrated that SN bifurcation is not possible in this case because the switching function $\sigma_{ss}(D)$ is monotone with respect to the duty cycle D. However, PD can take place in this converter if a suitable parameter is varied. One would be interested on determining the boundary in the parameter space of this instability. Figure 11 shows such a boundary in the parameter space (D, σ_e) for the system. It is worth noting that a traditional approximated approach will predict PD instability for duty cycle values larger than 0.5 in the case of not using a compensating ramp ($\sigma_e = 0$). Note that the exact closed-form expression predicts a lower critical value of the duty cycle ($D_c \approx 0.43$). Therefore, the approximated conventional approach could predict stability for a PWM system while it exhibits subharmonic oscillation due to PD bifurcation.

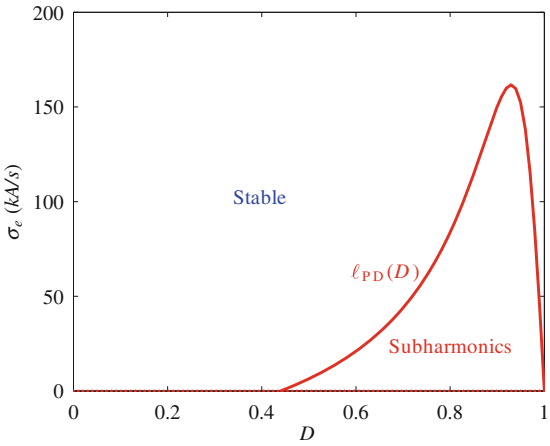

Fig. 11 PD bifurcation curve in terms of the duty cycle D and the slope σ_e of the compensating ramp for a boost converter under peak current mode control. The *curve* $\ell_{\mathrm{PD}}(D)$ represents the boundary

4.4.2 Special Linear Plants

The switched model for a PWM system with linear plant can be expressed in compact form as follows

$$\dot{\mathbf{x}} = \mathbf{A}\mathbf{x} + \mathbf{B}u + \mathbf{B}_2\mathbf{w}, \quad x_c = \mathbf{C}^{\mathsf{T}}(\mathbf{X}_{\mathrm{ref}} - \mathbf{x}) \tag{48}$$

where $\mathbf{B} = (\mathbf{B}_1 - \mathbf{B}_2)\mathbf{w}$. Let the Markov parameters of the system described by the 3-tuple $(\mathbf{A}, \mathbf{B}, \mathbf{C})$ as follows [27]

$$\mu_k = \mathbf{C}^{\mathsf{T}}\mathbf{A}^{k-1}\mathbf{B}, k = 1, 2.... \tag{49}$$

Hence, performing a Taylor series expansion on (46), the following equality holds at the onset of subharmonic instability

$$\begin{aligned}\sigma_{e,\mathrm{PD}}(D) &= \sum_{k=1}^{\infty} \mu_{k-1}\mathcal{S}_k(D)T^{k-1} \\ &\approx \mu_0(D - \frac{1}{2}) + \mu_1 T\left(\frac{D^2}{2} - \frac{D}{2} + \frac{1}{4}\right)\end{aligned} \tag{50}$$

The functions $\mathcal{S}_k(D)$ are related to the kth order Clausen polynomials $\mathrm{cl}_k(\theta)$ shown in Table 1 and having the following property [28].

$$\frac{\mathrm{d}}{\mathrm{d}\theta}\mathrm{cl}_k(\theta) = (-1)^k \mathrm{cl}_{k-1}(\theta) \quad \text{for}\, k = 2, 3\ldots \tag{51}$$

Moreover, the presence of these terms in (50) is largely dependent on the relative degree of the system (48) where the input is the command driving signal u and the

Table 1 Polynomial functions $\mathrm{cl}_k(\theta)$ and $\mathcal{S}_k(D)$

k	$\mathrm{cl}_k(\theta)$	$\mathcal{S}_k(D)$
1	$\frac{1}{2}(\pi-\theta)$	$D-\frac{1}{2}$
2	$\frac{\pi^2}{6}-\frac{\pi\theta}{2}+\frac{\theta^2}{4}$	$\frac{D^2}{2}-\frac{D}{2}+\frac{1}{4}$
3	$\frac{\pi^2\theta}{6}-\frac{\pi\theta^2}{4}+\frac{\theta^3}{12}$	$\frac{D^3}{6}-\frac{D^2}{4}+\frac{D}{12}$

output is the control signal x_c. The relative degree rd of a single-input single-output system is the smallest integer such that the Markov parameter $\mathbf{C}^\intercal\mathbf{A}^{rd-1}\mathbf{B}\neq 0$, i.e.,

$$rd=\inf\{k\geq 0:\mu_k\neq 0\} \tag{52}$$

The PWM system (plant including the controller) will have therefore a relative degree rd such that [27]

$$rd=1 \text{ if } \mu_0=\mathbf{C}^\intercal\mathbf{B}\neq 0, \tag{53a}$$

$$rd=2 \text{ if } \mu_0=\mathbf{C}^\intercal\mathbf{B}=0 \text{ and } \mu_1=\mathbf{C}^\intercal\mathbf{A}\mathbf{B}\neq 0 \tag{53b}$$

$$\vdots$$

Example 4: Let us apply the previous theoretical results to a buck converter with a simple proportional-integral (PI) control. The expressions of the matrix $\mathbf{A}$ and vector $\mathbf{B}$ are given by

$$\mathbf{A}=\begin{pmatrix}-\frac{1}{RC} & \frac{1}{C} & 0\\ -\frac{1}{L} & 0 & 0\\ -1 & 0 & 0\end{pmatrix},\quad \mathbf{B}=\begin{pmatrix}0\\ \frac{1}{L}\\ 0\end{pmatrix},\quad \mathbf{w}=v_g$$

The vector of the state variables after excluding the integrator is $\mathbf{x}(t)=(v_C,\ i_L)^\intercal$. Therefore, the vector $\mathbf{C}^\intercal=(k_v\ \ 0)$, where k_v is a voltage feedback gain. Figure 12 shows a schematic circuit diagram of a DC-DC buck converter under voltage mode PI control. All the parameters appearing in the matrices can be identified in the circuit diagram of Fig. 12. Because $\mathbf{A}_1=\mathbf{A}_2$, the plant is linear. The parameter values used are inductance $L=20$ mH, capacitance $C=47$ μF, lower value of the ramp modulator signal $V_l=3.8$ V, its amplitude $V_M=4.4$ V, switching period $T=400$ μs, voltage reference, $v_{\mathrm{ref}}=11.3$ V and voltage feedback gain $k_v=8.4$, [6, 19, 29].

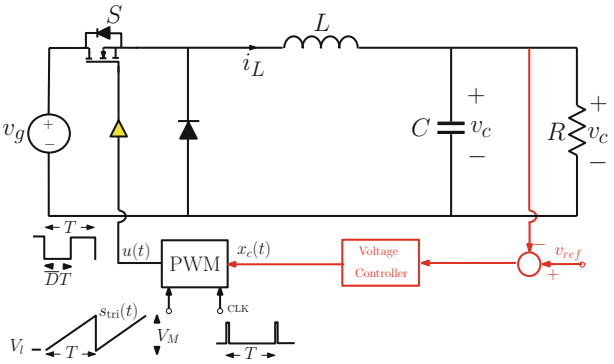

Fig. 12 Block circuit diagram of a DC-DC buck converter under PI voltage mode control

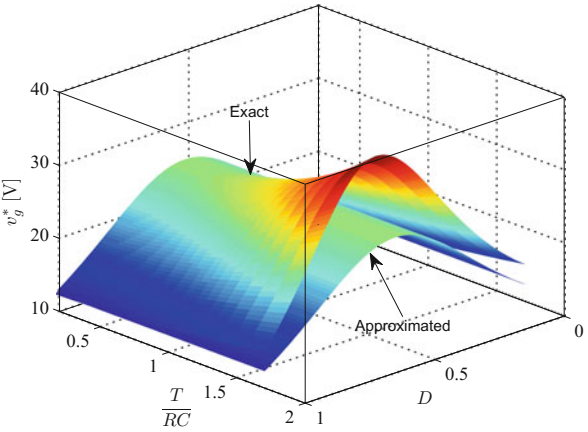

Fig. 13 Exact and approximated stability surface $v_g^*(T/(RC), D)$ in terms of the duty cycle D and $T/(RC)$ showing that only for high values of $T/(RC) \gg 1$ (not practical), (50) is not accurate enough

The control signal can be expressed as $x_c = \mathbf{C}^\intercal(\mathbf{X}_{\text{ref}} - \mathbf{x}) = k_v(v_{\text{ref}} - v_c)$. The time constant of the integrator is selected to be $\tau = 0.01$ s which is much larger than the switching period to ensure slow time-scale and to reduce its effects on the fast scale instability. Traditionally, the dynamic behavior of the system in this example has been studied in terms of the input voltage v_g and the load resistance R [6, 19, 29]. In Fig. 13, the exact mesh plot of the critical value of the input voltage $v_g^*(T/(RC), D)$ from (46) is shown together with the approximated plot from (50) using the first two terms in the expansion. From this figure, it can be observed that for $T/(RC) \ll 1$, a good concordance between the exact and the approximated expressions is obtained, while a discrepancy exists between their corresponding plots for relatively large values of $T/(RC)$. This discrepancy becomes significant for time constant RC approaching the switching period T. Only for $T/(RC) \gg 1$, (50) will give inaccurate results. However, this is not a practical case since the time constant of the converter filter must be much larger than the switching period in all practical implementations of switching converters in particular and PWM systems in general.

Finally, it should be noted that this example uses a LEM strategy and a change of variable $D \rightarrow (1 - D) := \overline{D}$ must be done in (46) together with a sign inversion in the voltage feedback gain.

5 Conclusions

In this chapter closed-form conditions for predicting the fast-scale stability boundaries corresponding to both saddle-node (SN) and period-doubling (PD) bifurcations have been derived for a class of PWM switching systems with bilinear plants. The results presented in this chapter can also be applied to the special case of switched systems with linear plants. Hence, for both cases, the effect of the different parameters of the system upon the stability boundary can be easily unveiled. The general-purpose derived expressions can be applied to different examples of PWM systems such as switching power converters, switched capacitor chaos generators, temperature control systems and hydraulic valve drive control among others. The stability boundaries have been derived without the need of the Jacobian matrix and without expressing the system trajectories in the Fourier frequency-domain and without any order reduction apart from excluding the integrator which has negligible effect on the fast scale instabilities. The simple asymptotic time-domain approach used in this chapter can be better understood by practitioners than those based in frequency-domain approach or on the eigenvalue problem of the Jacobian or the monodromy matrix.

Acknowledgments This work was supported by the Spanish *ministerio de Economía y Competitividad* under grant DPI2013-47437-R, the VPP of King Saud University, Riyadh, KSA and The Petroleum Institute, Abu Dhabi, UAE.

References

1. Liberzon, D. Switching in Systems and Control, Springuer, 2003
2. El Aroudi, A., Debbat, M., Martinez-Salamero, L.: Poincaré maps modelling and local orbital stability analysis of discontinuous piecewise affine periodically driven systems. Nonlinear Dyn. **50**(3), 431–445 (2007)
3. El Aroudi, A.: Prediction of subharmonic oscillation in switching converters under different control strategies. IEEE Trans. Circuits Syst. II: Express Briefs **62**(11), 910–914 (2014)
4. Fang, C.-C.: Using byquist or nyquist-like plot to predict three typical instabilities in DC-DC converters. J. Franklin Inst. **350**(10), 3293–3312 (2013)
5. Fang, C.-C.: Critical conditions for a class of switched linear systems based on harmonic balance: applications to DC-DC converters. Nonlinear Dyn. **70**(3), 1767–1789 (2012)
6. Giaouris, D., Maity, S., Banerjee, S., Pickert, V., Zahawi, B.: Application of Filippov method for the analysis of subharmonic instability in DC-DC converters. Int. J. Circuit Theory Appl. **37**(8), 899–919 (2009)
7. El Aroudi, A., Calvente, J., Giral, R., Martinez-Salamero, L.: Effects of non-ideal current sensing on subharmonic oscillation boundary in DC-DC switching converters under CMC.

In: Industrial Electronics Society, IECON 2013–39th Annual Conference of the IEEE, pp. 8367–8372, 10–13 Nov 2013
8. Fang, C.-C.: Critical conditions of saddle-node bifurcations in switching DC-DC converters. Int. J. Electron. **100**(8), 1147–1174 (2013)
9. Robert, B., Robert, C.: Border collision bifurcations in a one-dimensional piecewise smooth Map for a PWM current-programmed H-bridge Inverter. Int. J. Control **7**(16), 1356–1367 (2002)
10. Miladi, Y., Feki, M., Derbel, N.: On the model identification of an incubator based on genetic algorithms. In: 9th International Multi-Conference on Systems. Signals and Devices, Chemnitz, Germany (2012)
11. Gardini, L., Tramontana, F., Banerjee, S.: Bifurcation analysis of an inductorless chaos generator using 1D piecewise smooth map. Math. Comput. Simul. **95**, 137–145 (2014)
12. Huh J.-Y., Wennmacher, G.: A study on the stability analysis of a PWM controlled hydraulic equipment. KSME Int. J. **11**(4), 397–407 (1997)
13. Liu, G., Xia, W., Qi, D., Hu, R.: Analysis of Dither in electro-hydraulic proportional control. Telekominika **11**(11), 6808–6814 (2013)
14. Mandal, K., Chakraborty, C., Abusorrah, A., Al-Hindawi, M., Al-Turki, Y., Banerjee, S.: An automated algorithm for stability analysis of hybrid dynamical systems. Eur. Phys. J. Special Topics **222**, 757–768 (2013)
15. Mazumder, S.K., Nayfeh, A.H., Boroyevich, D.: Theoretical and experimental investigation of the fast- and slow-scale instabilities of a DC-DC converter. IEEE Trans. Power Electron. **16**(2), 201–216 (2001)
16. Leine, R.L., Nijemeijer, H.: Dynamics and Bifurcations of Non-smooth Mechanical Systems. Lecture Notes in Applied and Computational Mechanics, vol. 18. Springer, Heidelberg (2004)
17. Fang, C.-C., Abed, E.H.: Harmonic balance analysis and control of period doubling bifurcation in buck converters. IEEE Int. Symp. Circuits Syst. **3**, 209–212 (2001)
18. Hiskens, I.A., Pai, M.A.: Trajectory sensitivity analysis of hybrid systems. IEEE Trans. Circuits Syst. I: Fundam. Theory Appl. **47**(2), 204–220, (2000)
19. Fossas, E., Olivar, G.: Study of Chaos in the buck converter. IEEE Trans. Circuits Syst. I: Fundam. Theory Appl. **43**(1), 13–25 (1996)
20. El Aroudi, A.: A closed form expression for predicting fast scale instability in switching buck converters. In: The International Conference on Structural Nonlinear Dynamics and Diagnosis, Marrakech, Morocco (2012)
21. Tanitteerapan, T., Mori, S.: Fundamental frequency parabolic PWM controller for lossless soft-switching boost power factor correction. In: The 2001 IEEE International Symposium on Circuits and Systems, ISCAS 2001, vol. 3, pp. 57–60 (2001)
22. Fang, C.-C. Exact orbital stability analysis of static and dynamic ramp compensations in DC-DC converters. In: Proceedings IEEE International Symposium on Industrial Electronics, ISIE 2001, vol. 3, pp. 2124–2129 (2001)
23. Lehman, B., Bass, R.M.: Switching frequency dependent averaged models for PWM DC-DC converters. IEEE Trans. Power Electron. **11**(1), 89–98 (1996)
24. van der Woude, J.W., De Koning, W., Fuad, Y.: On the periodic behavior of PWM DC-DC converters. IEEE Trans. Power Electron. **17**(4), 585–595 (2002)
25. El Aroudi, A., Giaouris, D., Martinez-Salamero, L., Banerjee, S., Voutetakis, S., Papadopoulou, S.: Bifurcation behavior in switching converters driving other downstream converters in DC distributed power systems applications. In: MEDYNA'2013 Marrakech Morocco (2013)
26. El Aroudi, A.: A time-domain asymptotic approach to predict saddle-node and period doubling bifurcations in pulse width modulated piecewise linear systems. In: The International Conference on Structural Nonlinear Dynamics and Diagnosis, Agadir, Morocco (2014)
27. Corriou, J.-P.: Process control: theory and applications. Springer, London (2014). ISBN 978-1-4471-3848-8
28. Lewin, L.: Polylogarithms and Associated Functions. North-Holland, New York (1981)
29. Hamill, D.C., Deane, J.H.B., Jefferies, D.J.: Modelling of chaotic DC-DC converters by iterated nonlinear mapping. IEEE Trans. Power Electron. **7**(1), 25–36 (1992)